Adsorption 2, 33–40 (1996)

Binary Fluids in Planar Nanopores: Adsorptive Selectivity, Heat Capacity and Self-Diffusivity

SUSAN A. SOMERS*, K. GANAPATHY AYAPPA†, ALON V. McCORMICK AND H. TED DAVIS‡
Department of Chemical Engineering and Materials Science, University of Minnesota, Minneapolis, MN 55455

Abstract. Monte Carlo and molecular dynamics simulations are performed to study fluid adsorption of a two component fluid in slit pores of nanoscopic dimensions. The slit pores are immersed in a binary fluid bath, which is comprised of spherical molecules having a size ratio of 1.43, at constant temperature and composition. Pore width is varied to determine how the heat capacity and self-diffusion coefficient are linked to the composition and structure of the adsorbed fluid. In pores where the fluid structure is most pronounced, we observe: perfect (or near perfect) exclusion of one component by the other component, a heat capacity that rapidly oscillates and is of greater magnitude than in the fluid bath, and self-diffusion coefficients on the order of 10^{-8} cm^2/s. The behavior of the heat capacity and diffusion coefficients appears to arise from a near solid-like layering of OMCTS that occurs at certain favorable pore widths.

Keywords: binary adsorption, micropores, nanopores, molecular simulation

Introduction

In an earlier work (Somers et al., 1993), we described grand canonical Monte Carlo simulations of a binary fluid being adsorbed into slit micropores. In that report, we observed that the degree of selective adsorption varied rapidly with wall separation, in agreement with previous work (Vanderlick et al., 1991; MacElroy and Suh, 1987; Kierlik and Rosinberg, 1991; Tan and Gubbins, 1992). We also demonstrated that these rapid changes in selectivity were linked to the competing abilities of each component to form molecular layers between the pore walls; the component that was better able to pack as an integral number of layers was preferentially adsorbed. Furthermore, we found that preferential adsorption could result in complete selectivity, even in pores wide enough to admit either component (Somers et al., 1993). This feature had not been previously reported.

In this paper we investigate how the competition for pore space is reflected in the heat capacity and self-diffusivity of the adsorbed phase. We did this by performing Monte Carlo (MC) and molecular dynamics (MD) simulations of binary fluid adsorption in slit micropores ranging in width from 7.02 to 18.85 Å. As in our earlier study (Somers et al., 1993), we chose the simulation conditions to model slit micropores immersed in a fluid bath of cyclohexane and Octamethylcyclotetrasiloxane (OMCTS) at 30°C. To reduce computational cost, we ignored the atomic structure of the fluid molecules and pore walls, i.e., the fluid molecules were spherical and the pore walls were flat and smooth.

Description of Methods

A schematic of the slit pore system is shown in Fig. 1. As in Somers et al. (1993), we modeled the cyclohexane and OMCTS as spherical molecules obeying a Lennard-Jones 12-6 potential energy of interaction. For a pair of molecules i and j, this energy is given by

$$u_{ij} = 4\varepsilon_{ij}\left[\left(\frac{\sigma_{ij}}{r_{ij}}\right)^{12} - \left(\frac{\sigma_{ij}}{r_{ij}}\right)^{6}\right], \qquad (1)$$

where r_{ij} is the distance between molecules i and j, σ_{ij} is the effective molecular diameter of i and j, and ε_{ij}

*The Dow Chemical Company, 438 Building, Midland, MI 48667.
†Dept. of Chem. Eng., Indian Institute of Science, Bangalore, Karnataka, India 560012.
‡To whom correspondence should be addressed.

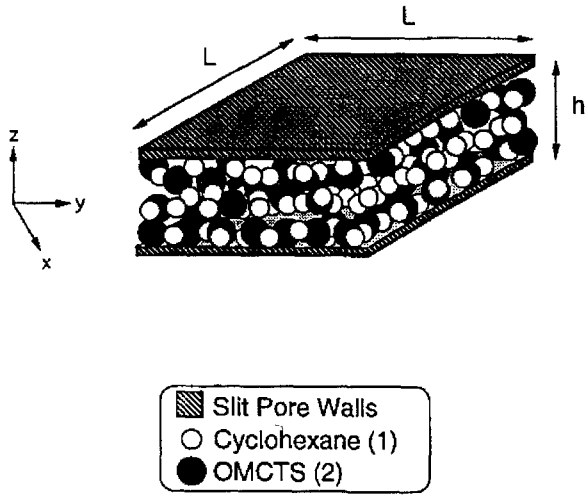

Figure 1. The slit pore system. h is the pore width and L is the side of the simulation cell. Although it is not shown in this figure, the pore walls extend to infinity in the x and y directions. This is because periodic boundary conditions were employed.

is the interaction strength of i and j (see Table 1). In calculating these interactions, we employed standard simulation techniques such as periodic boundary conditions and the minimum image convention (Allen and Tildesley, 1990). Consistent with these techniques, the fluid-fluid interaction potential was set to zero for a pair of molecules i and j when $r_{ij} = (x_{ij}^2 + y_{ij}^2)^{0.5}$ was greater than half the length, L, of the simulation box. A mean field correction to the potential energy was also calculated to account for residual interactions between molecules separated by more than the cutoff distance.

Along the z direction, the fluid was bound by atomically smooth slit pore walls. We used a 10-4-3 potential (Somers et al., 1993) to model interactions of the fluid with the pore walls. For this potential, the interaction between one pore wall and a fluid molecule of type i located at position z_i in the pore is

$$\Psi_{iw}(z_{iw}) = 2\pi\rho_s\varepsilon_{iw} \times\left\{\sum_{k=0}^{3}\left[\frac{2\sigma_{iw}^{12}}{5(z_{iw}+k\Delta z)^{10}} - \frac{\sigma_{iw}^{6}}{(z_{iw}+k\Delta z)^{4}}\right] - \frac{\sigma_{iw}^{6}}{3\Delta z_{\text{far}}(z_{iw}+3\Delta z+\Delta z_{\text{far}})^{3}}\right\},$$

where

$$z_{iw} = \left\{\begin{array}{ll}\left|z_i + \dfrac{h}{2}\right| & \text{wall at } z = -\dfrac{h}{2} \\ \left|z_i - \dfrac{h}{2}\right| & \text{wall at } z = \dfrac{h}{2}\end{array}\right\}, \quad -h/2 \le z_i \le h/2. \tag{2}$$

Here z_{iw} is the perpendicular distance between the center of the fluid molecule and the center of the layer of atoms lining the pore wall, σ_{iw} is the effective fluid-wall molecular diameter, ε_{iw} is the effective fluid-wall interaction energy, $\rho_S = 0.12$ Å^{-2} is the surface density of the pore wall atoms, and $\Delta z = 2.2$ Å and $\Delta z_{\text{far}} = 2.5$ Å are wall lattice distance parameters. Further details may be found in (Somers et al., 1993).

We performed all the simulations described in this paper for slit pores having a fixed temperature (30°C), volume, and number of adsorbates. We met these conditions in the MC simulations by performing our calculations in the Canonical ensemble (Allen and Tildesley, 1990; Hill, 1986). In the MD simulations, we used a leap-frog algorithm having a time step of 0.0836 ps to numerically solve the equations of motion for the fluid molecules with time. Within this algorithm, we maintained isothermal conditions by scaling the thermal velocities of the fluid molecules (Allen and Tildesley, 1990).

Table 1. Lennard-Jones parameters[a].

	Cyclohexane (species = 1)	OMCTS (species = 2)	Wall atoms (species = w)
Molecular diameter (σ)	5.4 Å[b]	7.7 Å[b]	2.71 Å
Interaction strength (ε)	4.473×10^{-14} erg	4.736×10^{-14} erg	1.629×10^{-14} erg

[a]In Eq. (1), $\sigma_{ij} = 0.5(\sigma_i + \sigma_j)$ and $\varepsilon_{ij} = (\varepsilon_i\varepsilon_j)^{1/2}$, where i and j equal 1 or 2. These same mixing rules apply in Eq. (2), where i equals 1 or 2 and j equals w. See Somers et al. (1993) for more details.

[b]Molecular diameters of Cyclohexane and OMCTS were calculated from the solvation forces of pure fluids, as measured in surface forces experiments (Vanderlick et al., 1991).

Table 2a. Simulation conditions for pores immersed in the 42 mole percent cyclohexane bath.

Pore width $[h(\sigma_1)]$	Mean pore density of cyclohexane $[\rho(\sigma_1^{-3})]$	Mean pore density of OMCTS $[\rho(\sigma_2^{-3})]$
1.3	0.296	0
1.35	0.593	0
1.5	0.599	0
1.63	0.552	0
1.75	0	0.832
2.0	0	0.728
2.13	0	0.678
2.25	0	0.618
2.5	0.251	0.432
2.75	0.224	0.539
3.0	0.0017	0.849
3.25	0	0.823
3.5	0.017	0.745
3.75	0.107	0.644
3.88	0.129	0.685
4.0	0.137	0.664
4.25	0.098	0.719
4.5	0.006	0.739
4.63	0.012	0.854
4.75	0.035	0.78
5	0.060	0.725
5.25	0.114	0.687
5.5	0.111	0.696
5.75	0.089	0.722
6.0	0.072	0.745
14.5	0.128	0.652
Bath	0.156	0.612

Table 2b. Simulation conditions for pores immersed in the 85 mole percent cyclohexane bath.

Pore width $[h(\sigma_1)]$	Mean pore density of cyclohexane $[\rho(\sigma_1^{-3})]$	Mean pore density of OMCTS $[\rho(\sigma_2^{-3})]$
1.35	0.630	0
1.7	0.361	0.243
1.75	0.051	0.713
2.0	0.011	0.690
2.1	0.015	0.655
2.25	0.304	0.342
2.38	0.641	0.055
2.5	0.520	0.171
2.75	0.323	0.423
3.0	0.208	0.849
3.25	0.083	0.693
3.38	0.125	0.638
3.5	0.280	0.467
3.75	0.319	0.435
4.0	0.300	0.464
4.25	0.255	0.512
4.5	0.236	0.394
5	0.228	0.302
Bath	0.496	0.255

The mean density in each pore was chosen equal to the mean density calculated previously from Grand Canonical Monte Carlo simulations of the same slit pore system (Somers et al., 1993). These mean densities (given in Tables 2a and 2b) correspond to those in pores immersed in a fluid bath at 30°C and of either 42 or 85 mole percent cyclohexane. Strictly speaking, the mean fluid density in a pore that is immersed in a fluid bath can fluctuate. We did not model such fluctuations, however, since MD simulations are more readily applied and the heat capacity is more accurately calculated when the mean density is fixed (Karavias and Myers, 1991).

To speed up equilibration of the MC and MD simulations, we selected the molecular coordinates from previously equilibrated Grand Canonical Monte Carlo simulations (Somers et al., 1993) for the starting configuration of the fluid molecules. For both simulations, it was decided that equilibrium was reached when the total system energy remained steady. After the simulations were equilibrated, heat capacities were calculated over 6 to 14 million MC steps, while diffusion coefficients were calculated during MD simulations ranging from 40 to 75 thousand time steps.

Results and Discussion

Heat Capacity

By definition, the heat capacity is related to the total energy by

$$C_V \equiv \frac{\partial\langle U+K\rangle}{\partial T} = \frac{\partial\langle U\rangle}{\partial T} + \frac{3}{2}NK_b, \qquad (3)$$

where the brackets represent ensemble averages, U is the potential energy, K is the kinetic energy, T

is the temperature, $N = N_1 + N_2$ is the total number of cyclohexane and OMCTS molecules adsorbed in the simulation cell (Fig. 1), and k_b is Boltzmann's constant. The second part of this relation holds for a fluid at a fixed temperature and number of particles (where $\langle K \rangle = \frac{3}{2} N K_b T$). The partial derivative of $\langle U \rangle$ with respect to temperature can be evaluated from statistical thermodynamics (Hill, 1986), so that upon rearrangement one gets

$$\frac{C_V}{Nk_b} = \frac{\langle U^2 \rangle - \langle U \rangle^2}{N(k_b T)^2} + \frac{3}{2}. \tag{4}$$

It is clear from this relation that the potential energy contribution to the heat capacity arises from dispersion of the potential energy about its mean. We calculated this term directly in the MC simulations by averaging U^2 and U over each fluid configuration in a Markov chain (Allen and Tildesley, 1990).

In Figs. 2a and 2b, the heat capacity of the adsorbed fluid (calculated from Eq. 4) is shown as a function of pore width. Error bars are displayed when the standard deviation of the heat capacity about its mean (calculated from more than one MC simulation) is greater than the size of the drawn data points. The pore averaged composition of cyclohexane is also given in these figures, and the heat capacity of the bath fluid is drawn as a horizontal line.

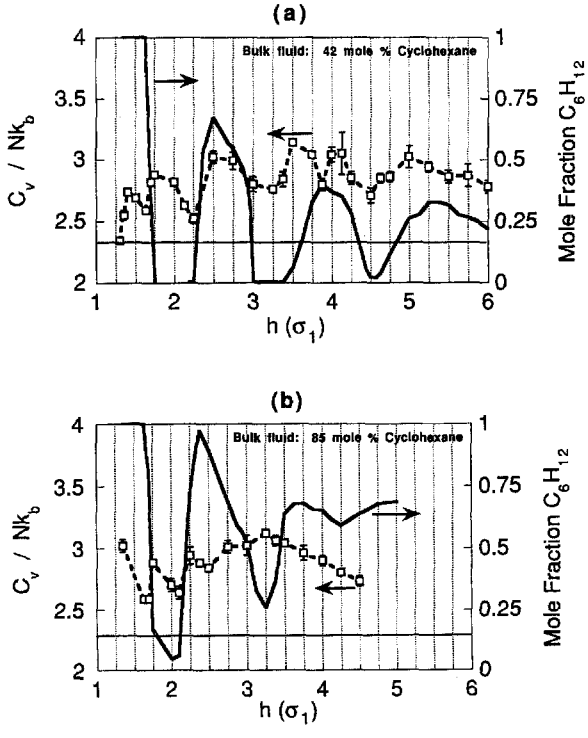

Figure 2. Heat capacity (- - - -) and cyclohexane mole fraction (—) versus pore width at bulk cyclohexane mole fractions of (a) 42 and (b) 85 percent.

To test the accuracy of the simulations, we calculated the heat capacity in pores of width 2.25 and $2.5\sigma_1$ (in the OMCTS rich bath) using the definition in Eq. (3). To do this, we performed MC simulations and calculated the total potential energy, $\langle U \rangle$, at temperatures of 27, 30, 33 and 35°C. Next, we performed a least squares fit on the resulting energy and temperature data, numerically differentiated the result to obtain $\frac{\partial \langle U \rangle}{\partial T}|_{N,V}$ and substituted this value into Eq. (3). The heat capacity calculated from this technique was $2.4Nk_b$ for $h = 2.25\sigma_1$ and $3.1Nk_b$ for $h = 2.5\sigma_1$. This compares well with the heat capacity calculated from Eq. (4), namely $2.52Nk_b$ for $h = 2.25\sigma_1$ and $3.02Nk_b$ for $h = 2.5\sigma_1$.

One obvious feature of the heat capacity is that it oscillates rapidly with pore width, especially below $h = 4.5\sigma_1$ in the OMCTS rich bath and below $h = 2.5\sigma_1$ in the OMCTS poor bath. At first glance, it appears that these oscillations are linked to changes in the pore fluid composition. However, MC simulations for bulk fluids (where the boundary conditions were triply periodic and there were no external potentials) at a variety of cyclohexane/OMCTS mole fractions showed that the heat capacity was nearly constant with composition (Table 3). Thus, changes in the pore fluid composition are unlikely to be the main cause of the heat capacity oscillations.

The rapid oscillations in the heat capacity are more likely linked to the strong layering structure of the confined fluid. The oscillations exist in the same range of pore widths where very high adsorptive selectivity occurs (i.e., in pores narrower than $4.5\sigma_1$ when immersed in the OMCTS rich bath and $2.5\sigma_1$ when immersed in the cyclohexane rich bath). Recall that high selectivity coincided with strong layering of the selected component (Somers et al., 1993).

Along with this, the heat capacity of the adsorbed fluid is as much as $0.84Nk_b$ higher than that of the bath fluid. Our interpretation is that this added heat capacity arises from the vibrational modes of the highly confined and layered fluid structures that form near the pore walls (Fig. 3). In each direction, translation contributes $0.5k_b$ per molecule to the heat capacity, while vibration contributes k_b per molecule. Therefore, whenever a

Table 3. Bulk fluid and wide pore results.

	Heat capacity (Nk_b)	Self-diffusivity (10^{-5} cm^2/s)
Pure cyclohexane	2.23 ± 0.01[a]	1.43[b]
85 Mole% cyclohexane	2.28 ± 0.06	—
42 Mole% cyclohexane	2.32 ± 0.02	Cyclohexane: 1.49 ± 0.00
		OMCTS: 0.87 ± 0.02
Pure OMCTS	2.31 ± 0.01	0.94[b]
Pore of width $14.5\sigma_1$ (Bath is 42 Mole% cyclohexane)	2.56 ± 0.03	Cyclohexane: 1.32 ± 0.01
		OMCTS: 0.65 ± 0.02

[a]The experimental result for the heat capacity of pure cyclohexane at 30°C is approximately $25Nk_b$ (Weast, 1982). This value is larger than the heat capacity we calculated. This is because the fluid molecules in our model were spheres and, hence did not have internal or rotational degrees of freedom which contribute to the heat capacity of the experimental fluids.

[b]Self-diffusivities in pure cyclohexane and in pure OMCTS were calculated using an empirical equation for pure Lennard-Jones bulk fluids (Levesque and Verlet, 1970).

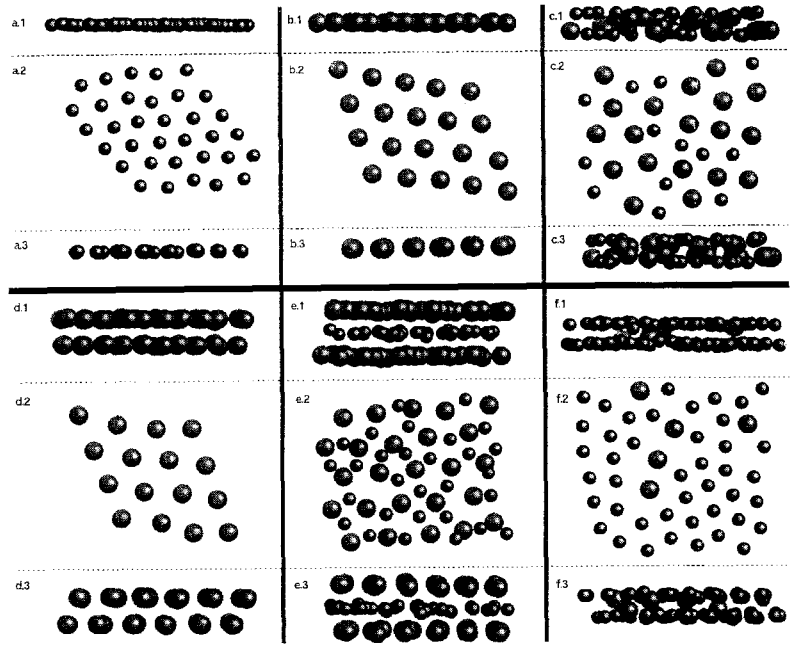

Figure 3. Snapshots of fluid particle configurations for one MC configuration (a) $h = 1.35\sigma_1$, (b) $h = 1.75\sigma_1$, (c) $h = 2.5\sigma_1$, (d) $h = 3.0\sigma_1$, (e) $h = 3.88\sigma_1$, and (f) $h = 2.38\sigma_1$. Note: The bath fluid composition is 42 mole percent cyclohexane in (a–e) and 85 mole percent cyclohexane in (f). The smaller spheres are cyclohexane and the larger spheres are OMCTS. In the snapshots, x.1 and x.3 denote views where the planar walls (not shown) are perpendicular to the page (i.e., walls above and below each figure) and x.2 denotes views where the planar walls (not shown) are parallel to the page (i.e., walls above and below the page).

molecule vibrates instead of translates, it contributes an extra $0.5k_b$ (per direction) to the ensemble average of the heat capacity.

As expected, the heat capacity of the fluid adsorbed in a pore of width $14.5\sigma_1$ is only ten percent higher than that of the bath fluid (Table 3). In this wider pore, a lower percentage of fluid molecules interacts strongly with the walls. As a result, pronounced fluid order is mainly confined to the region of the pore near the walls, and the adsorbed fluid is more bulk-like.

Self-Diffusivity

We used two methods to calculate the effective self-diffusivity of each species. In one method, we calculated the self-diffusivity from the Einstein relationship:

$$D_i = \frac{1}{4}\lim_{\tau^E\to\infty}\frac{d}{dt}\langle x(t=0)x(t=\tau^E) + y(t=0)y(t=\tau^E)\rangle_i, \tag{5}$$

where $i = 1$ denotes cyclohexane, $i = 2$ denotes OMCTS, and the term in brackets is the ensemble average of the mean squared displacement for species i along directions parallel to the pore walls (x and y). This relationship holds for τ^E such that the mean squared displacement is linear with time; i.e., it holds when the self-diffusion coefficient (D_i) is constant with time. In our simulations, $\tau^E = 110$ ps, except at $h = 3.25\sigma_1$ where it was 220 ps. To calculate the ensemble averaged mean squared displacement of species i, we performed averages over both time origins (i.e., $t = 0$) and the total number of molecules for species i (N_i):

$$\langle x(t=0)x(t=\tau^E) + y(t=0)y(t=\tau^E)\rangle_i = \frac{\sum_{j=1}^{N_{\text{Origins}}}\sum_{k=1}^{N_i} x_k(t=t_j)x_k(t=t_j+\tau^E)+y_k(t=t_j)y_k(t=t_j+\tau^E)}{N_{\text{Origins}}N_i}. \tag{6}$$

Here, x_k and y_k are the $x - y$ coordinates of the kth fluid particle, and N_{Origins} is the number of time origins summed over. The shifting of time origins in Eq. (6) is valid provided the mean squared displacement is stationary with time, which it is for a fluid at equilibrium.

If τ^E is not large enough, the mean squared displacement can lead to erroneous diffusivity values. Because of this, we also calculated the self-diffusivity of each component using the Green-Kubo relation

$$D_i = \frac{1}{2}\int_0^{\tau^{\text{GK}}} \langle v_x(t=0)v_x(t=t') + v_y(t=0)v_y(t=t')\rangle_i\, dt', \tag{7}$$

where the bracketed expression is the ensemble averaged velocity autocorrelation function for species i along directions parallel to the pore walls. τ^{GK} was chosen such that contributions to the integral approached zero for $t' > \tau^{\text{GK}}$. Here, τ^{GK} was 40 ps, except at $h = 1.75\sigma_1$ and $14.5\sigma_1$ where it was 20 ps. As above, the ensemble average was performed over both time origins and species i particles

$$\langle v_x(t=0)v_x(t=t') + v_y(t=0)v_y(t=t')\rangle_i = \frac{\sum_{j=1}^{N_{\text{Origins}}}\sum_{k=1}^{N_i} v_{x,k}(t=t_j)v_{x,k}(t=t_j+t')+v_{y,k}(t=t_j)v_{y,k}(t=t_j+t')}{N_{\text{Origins}}N_i}, \tag{8}$$

where $v_{x,k}$ and $v_{y,k}$ are the $x - y$ velocity components for the kth fluid particle.

Figures 4a and 4b show the self-diffusivities of cyclohexane and OMCTS, reported as a percentage of the bulk fluid self-diffusion coefficients (the bulk fluid contained 42 mole percent cyclohexane). The plotted diffusion coefficients are averages over the values obtained by each of the two methods described above. Error bars are drawn when the standard deviation from the average was greater then the size of the drawn data points (the methods are in good agreement, except at $h = 3.0\sigma_1$). In Fig. 4a, we set the self-diffusivity of cyclohexane to zero at pore widths of 2.25 and $3.25\sigma_1$, because it was not adsorbed by those pores. The horizontal lines in Fig. 4 represent diffusion coefficients equal to 5×10^{-6} and 5×10^{-7} cm^2/s and are drawn as a visual aid.

Table 3 shows that the self-diffusion coefficients for cyclohexane and OMCTS in the fluid bath are on the order of 10^{-5} cm^2/s, as expected for a liquid. This is also true for the pore that is $14.5\sigma_1$ wide, where the diffusivities for cyclohexane and OMCTS are roughly 89 and 75 percent of their bath fluid values, respectively. As shown by Fig. 4, the self-diffusivities in narrower pores are markedly lower, so much so that the self-diffusion coefficient is liquid-like *only for cyclohexane* (at $h = 3.0$, $h = 3.88$, and $h > 4.5\sigma_1$).

The self-diffusion coefficient is least (near 10^{-8} cm^2/s) in pores where high selectivity exists. Meaning that, these low self-diffusivities are accompanied by

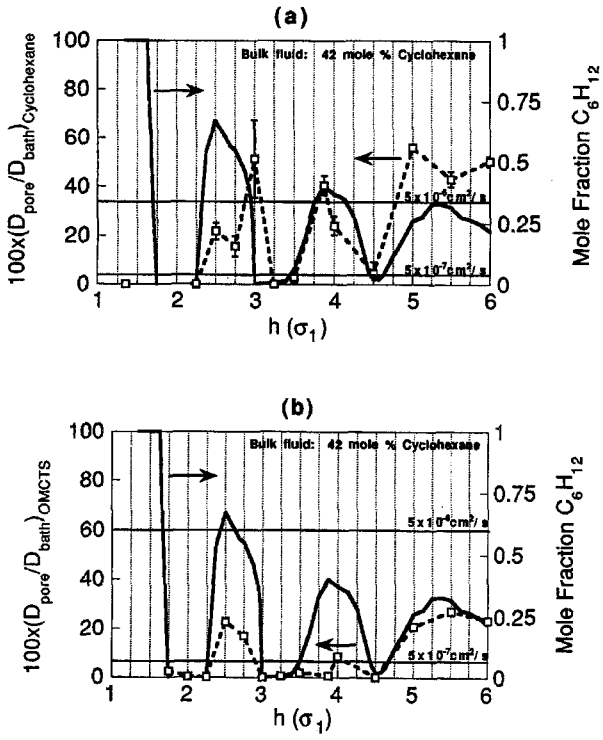

Figure 4. Pore fluid self-diffusion coefficient as a percentage of the bulk fluid self-diffusion coefficient (- - - -) and cyclohexane mole fraction (—) versus pore width at bulk cyclohexane mole fractions of 42 mole percent. Self-diffusion coefficients are of (a) cyclohexane and (b) OMCTS.

strongly ordered, like-molecular layers (see Fig. 3 and Somers et al., 1993). We do not have a good estimate for the self-diffusion coefficient in solids, which varies by over 10 orders of magnitude in different systems. However, in soft solids it is often about 10^{-8} cm^2/s or somewhat lower (Cussler, 1987). Thus, the observed high adsorbate selectivity is likely to be linked to a layering order approaching crystallization.

For example, the self-diffusivities for OMCTS are least when packing of one (near $h = 2.0\sigma_1$) or two (near $h = 3.0\sigma_1$) layers of OMCTS is so overwhelmingly preferred that cyclohexane is not adsorbed (Figs. 3b and 3d). The same holds near $h = 4.5\sigma_1$, where three layers of OMCTS are preferred. A notable exception to this trend occurs at a pore width of $3.88\sigma_1$, where the self-diffusivity of OMCTS is low even though the pore is not highly selective. In this case, Fig. 3e shows that a very well developed monolayer of OMCTS is adsorbed at each wall and a less well defined, more mobile layer of cyclohexane forms between them. Thus, again the OMCTS self-diffusivity is low because the OMCTS molecules reside in highly ordered layers. For cyclohexane, the self-diffusivity is low when molecular sieving does not permit OMCTS to enter the pore (near $h = 1.35\sigma_1$, see Fig. 3a) and when OMCTS layering virtually shuts out cyclohexane from the porespace.

As an added note, we measured the self-diffusivities in a pore of width $2.38\sigma_1$ immersed in a bath of 85 mole percent cyclohexane. The self-diffusion coefficients for cyclohexane and for OMCTS were approximately 0.2×10^{-5} cm^2/s. These liquid-like values were present despite the very high selectivity for cyclohexane (Fig. 2b) and the layering of cyclohexane molecules in this pore (Fig. 3f). Here, the OMCTS molecules adsorbed at the pore center disrupted the ordering of cyclohexane molecules along the pore walls (Fig. 3f.2), so the diffusion coefficients were not solid-like. Recall that cyclohexane, which was the species highly selected in this pore, had weaker interactions with the pore walls than did OMCTS.

Summary

Competition between components for pore space in an adsorbed binary fluid affects not only the order and composition of the adsorbed fluid, but also the heat capacity and mobility of that fluid.

The heat capacity oscillates rapidly with pore width. These oscillations occur in the same range of pore widths where the competing abilities of each species to form like-molecule layers result in high selectivity, even in complete selectivity for some cases. In addition, the heat capacity of the pore fluid is higher than in the bath because of the increased molecular order in the pore.

The self-diffusion coefficient oscillates with pore width in a manner closely linked to the adsorbed fluid composition. The self-diffusivity is solid-like in pores where high selectivity and like-molecule layering (Somers et al., 1993) exist. Thus, although high selectivity in pores wide enough to admit either component is encouraging for industrial applications, the low diffusivities imply that additional work must be done to make this a viable separations technique. On a more promising note, the diffusivity is not solid-like for a pore selectively adsorbing cyclohexane in a cyclohexane rich bath. This suggests that more feasible separations might be accomplished by reducing the affinity of the pore to each species.

Acknowledgments

Computational resources on the Cray-2 and Cray-XMP were granted by the University of Minnesota Supercomputer Institute.

References

Allen, M.P. and D.J. Tildesley, *Computer Simulation of Liquids*, Clarendon Press, Oxford, 1990.

Cussler, E.L., *Diffusion: Mass Transfer in Fluid Systems*, Cambridge University Press, Cambridge, 1987.

Hill, T.L., *An Introduction to Statistical Thermodynamics*, Dover Publications, New York, 1986.

Karavias, F. and A.L. Myers, "Isoteric Heats of Multicomponent Adsorption: Thermodynamics and Computer Simulations," *Langmuir*, **7**, 3118 (1991).

Kierlik, E. and M.L. Rosinberg, "Density-Functional Theory for Inhomogeneous Fluids: Adsorption of Binary Mixtures," *Phys. Rev. A*, **44**, 5025 (1991).

Levesque, D. and L. Verlet, "Computer 'Experiments' on Classical Fluids. III Time-Dependent Self-Correlation Functions," *Phys. Rev. A*, **2**, 2514 (1970).

MacElroy, J.M.D. and S.-H. Suh, "Computer Simulation of Moderately Dense Hard-Sphere Fluids and Mixtures in Microcapillaries," *Mol. Phys.*, **60**, 475 (1987).

Somers, S.A., A.V. McCormick, and H.T. Davis, "Superselectivity and Solvation Forces of a Two Component Fluid Adsorbed in Slit Micropores," *J. Chem. Phys.*, **99**, 9890 (1993).

Tan, Z. and K.E. Gubbins, "Selective Adsorption of Simple Mixtures in Slit Pores: A Model of Methane-Ethane Mixtures in Carbon," *J. Phys. Chem.*, **96**, 845 (1992).

Vanderlick, T.K., L.E. Scriven, and H.T. Davis, "Forces Bbtween Solid Surfaces in Binary Solutions," *Colloids and Surfaces*, **52**, 9 (1991).

Weast, R.V. (Ed.), *Handbook of Chemistry and Physics*, CRC Press, Boca Raton, 1982.